Calculating the Magnetic Anisotropy of Rare-Earth–Transition-Metal Ferrimagnets

Christopher E. Patrick,[1,*] Santosh Kumar,[1] Geetha Balakrishnan,[1] Rachel S. Edwards,[1]
Martin R. Lees,[1] Leon Petit,[2] and Julie B. Staunton[1]
[1]*Department of Physics, University of Warwick, Coventry CV4 7AL, United Kingdom*
[2]*Daresbury Laboratory, Daresbury, Warrington WA4 4AD, United Kingdom*

(Received 13 November 2017; published 28 February 2018)

Magnetocrystalline anisotropy, the microscopic origin of permanent magnetism, is often explained in terms of ferromagnets. However, the best performing permanent magnets based on rare earths and transition metals (RE-TM) are in fact *ferri*magnets, consisting of a number of magnetic sublattices. Here we show how a naive calculation of the magnetocrystalline anisotropy of the classic RE-TM ferrimagnet $GdCo_5$ gives numbers that are too large at 0 K and exhibit the wrong temperature dependence. We solve this problem by introducing a first-principles approach to calculate temperature-dependent magnetization versus field (FPMVB) curves, mirroring the experiments actually used to determine the anisotropy. We pair our calculations with measurements on a recently grown single crystal of $GdCo_5$, and find excellent agreement. The FPMVB approach demonstrates a new level of sophistication in the use of first-principles calculations to understand RE-TM magnets.

DOI: 10.1103/PhysRevLett.120.097202

High-performance permanent magnets, as found in generators, sensors and actuators, are characterized by a large volume magnetization and a high coercivity [1]. The coercivity—which measures the resistance to demagnetization by external fields—is upper-bounded by the material's magnetic anisotropy [2], which in qualitative terms describes a preference for magnetization in particular directions. Magnetic anisotropy may be partitioned into two contributions: the shape anisotropy, determined by the macroscopic dimensions of the sample, and the magnetocrystalline anisotropy (MCA), which depends only on the material's crystal structure and chemical composition. Horseshoe magnets provide a practical demonstration of shape anisotropy, but the MCA is less intuitive, arising from the relativistic quantum mechanical coupling of spin and orbital degrees of freedom [3].

Permanent magnet technology was revolutionized with the discovery of the rare-earth–transition-metal (RE-TM) magnet class, beginning with Sm-Co magnets in 1967 [4] (whose high-temperature performance is still unmatched [5]), followed by the world-leading workhorse magnets based on Nd-Fe-B [6,7]. With the TM providing the large volume magnetization, careful choice of RE yields MCA values which massively exceed the shape anisotropy contribution [8]. RE-TM magnets are now indispensable to everyday life, but their significant economic and environmental cost has inspired a global research effort aimed at replacing the critical materials required in their manufacture [9].

In order to perform a targeted search for new materials it is necessary to fully understand the huge MCA of existing RE-TM magnets. An impressive body of theoretical work based on crystal field theory has been built up over decades [10], where model parameters are determined from experiment (e.g., Ref. [11]) or electronic structure calculations [12–14]. An alternative and increasingly more common approach is to use these electronic structure calculations, usually based on density-functional theory (DFT), to calculate the material's magnetic properties directly, without referring to the crystal field picture [15–19].

Calculating the MCA of RE-TM magnets presents a number of challenges to electronic structure theory. The interaction of localized RE-4f electrons with their itinerant TM counterparts is poorly described within the most widely-used first-principles methodology, the local spin-density approximation (LSDA) [12]. Indeed, the MCA is inextricably linked to orbital magnetism, whose contribution to the exchange-correlation energy is missing in spin-only DFT [20,21]. MCA energies are generally a few meV per formula unit, necessitating a very high degree of numerical convergence [22]. Finally, the MCA depends strongly on temperature, so a practical theory of RE-TM magnets must go beyond zero-temperature DFT and include thermal disorder [23].

Even when these significant challenges have been overcome, there is a more fundamental problem. Experiments access the MCA indirectly, measuring the change in magnetization of a material when an external field is applied in different directions. By contrast, calculations usually access the MCA directly by evaluating the change in energy when the material is magnetized in different directions, with no reference to an external field. These experimental and computational approaches arrive at the same MCA energy, provided one is studying

a *ferro*magnet. However, the majority of RE-TM magnets (and many other technologically-important magnetic materials) are *ferri*magnets; i.e., they are composed of sublattices with magnetic moments of distinct magnitudes and orientations. Crucially, the application of an external field may introduce canting between these sublattices, affecting the measured magnetization. Thus, the standard theoretical approach of ignoring the external field is hard to reconcile with real experiments on ferrimagnets.

In this Letter, through a combination of calculations and experiments, we provide the hitherto missing link between electronic structure theory and practical measurements of the MCA. Specifically, we show how to directly simulate experiments by calculating, from first principles (FP), how the measured magnetization (M) varies as a function of field (B) applied along different directions and at different temperatures. We apply our first-principles magnetization versus field (FPMVB) approach to the RE-TM ferro and ferrimagnets YCo_5 and $GdCo_5$, which are isostructural to the technologically-important magnet $SmCo_5$ [24] and, in the case of $GdCo_5$, a source of controversy in the literature [25–35]. Pairing FPMVB with new measurements of the MCA of $GdCo_5$ allows us to resolve this controversy. More generally, FPMVB enables a new level of collaboration between theory and experiment in understanding the magnetic anisotropy of ferrimagnetic materials.

The electronic structure theory behind FPMVB treats magnetic disorder at a finite temperature T within the disordered local moment (DLM) picture [36,37]. The methodology allows the calculation of the magnetization of each sublattice i, $\boldsymbol{M_i}(T) = M_i(T)\hat{\boldsymbol{M}}_{\boldsymbol{i}}$, and the torque quantity $\partial F(T)/\partial\hat{\boldsymbol{M}}_{\boldsymbol{i}}$, where F is an approximation to the temperature dependent free energy. $\partial F(T)/\partial\hat{\boldsymbol{M}}_{\boldsymbol{i}}$ accounts for the anisotropy arising from the spin-orbit interaction, while the contribution from the classical magnetic dipole interaction is computed numerically [38]. Many of the technical details of the DFT-DLM calculations [36,39–43] were described in our recent study of the magnetization of the same compounds [44]; the extensions to calculate the torques are described in Ref. [37]. The Gd-4f electrons are treated with the local self-interaction correction [43], and we have also implemented the orbital polarization correction [20] following Refs. [45,46] using reported Racah parameters [47]. Details are given as Supplemental Material (SM) [48].

YCo_5 and $GdCo_5$ crystallize in the $CaCu_5$ structure, consisting of alternating hexagonal $RECo_{2c}/Co_{3g}$ layers [24]. Y is nonmagnetic, while in $GdCo_5$ the large spin moment of Gd (originating mainly from its half filled 4f shell) aligns antiferromagnetically with the Co moments. We now consider a "standard" calculation of the MCA based on a rigid rotation of the magnetization. If the Gd and Co moments are held antiparallel, $GdCo_5$ is effectively a ferromagnet with reduced moment $M_{\mathrm{Co}} - M_{\mathrm{Gd}}$. Then, from the hexagonal symmetry, we expect the angular dependence of the free energy to follow $\kappa_1 \sin^2\theta + \kappa_2 \sin^4\theta + \mathcal{O}(\sin^6\theta)$, where θ is the polar angle between the crystallographic c axis and the magnetization direction. The constants κ_1, κ_2 determine the change in free energy ΔF, calculated, e.g., from the force theorem [49] or the torque $dF/d\theta$ [50].

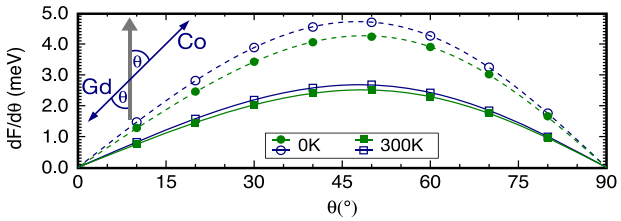

FIG. 1. Data points and fits of $dF/d\theta$ calculated for $GdCo_5$ (blue, empty symbols; Gd and Co moments held antiparallel) and YCo_5 (green, filled symbols), at 0 and 300 K.

In Fig. 1, we show $dF/d\theta$ calculated for ferromagnetic YCo_5 and $GdCo_5$ at 0 and 300 K. Fitting the data to the derivative of the textbook expression, $\sin 2\theta(\kappa_1 + 2\kappa_2 \sin^2\theta)$, finds κ_1 and κ_2 to be positive (easy c axis) with κ_1 an order of magnitude larger than κ_2. Considering experimentally measured anisotropy constants in the literature, for YCo_5, our κ_1 value of 3.67 meV (all energies are per formula unit, FU) at 0 K compares favorably to the values of 3.6 and 3.9 meV reported in Refs. [28,51]. At 300 K, our value of 2.19 meV exhibits a slightly faster decay with temperature compared to experiment (2.6 and 3.0 meV), which we attribute to our use of a classical spin Hamiltonian in the DLM picture [36,44]. However, for $GdCo_5$, our calculated values of κ_1 show very poor agreement with the experiments [26,29]. First, at 0 K, we find κ_1 to be larger than YCo_5 (4.26 meV), while experimentally the anisotropy constant is much smaller (1.5, 2.1 meV). Second, we find κ_1 decreases with temperature (2.39 meV at 300 K), while experimentally the anisotropy constant *increases* (2.7, 2.8 meV).

To understand these discrepancies, we must ask how the anisotropy energies were actually measured. Torque magnetometry provides an accurate method of accessing the MCA [52], but it is technically challenging in RE-TM magnets, which require very high fields to reach saturation [53]. Singular point detection [54] and ferromagnetic resonance [55] has also been used to investigate the MCA of polycrystalline and thin-film samples. However, the most commonly-used method for RE-TM magnets, employed in Refs. [26,29], is based on the seminal 1954 work by Sucksmith and Thompson [56] on the anisotropy of hexagonal ferromagnets. This work provides a relation between the measured magnetization M_{ab} and field B applied in the hard plane in terms of κ_1, κ_2 and the easy axis magnetization M_0 [48,56]:

$$(BM_0/2)/(M_{\mathrm{ab}}/M_0) \equiv \eta = \kappa_1 + 2\kappa_2(M_{\mathrm{ab}}/M_0)^2. \quad (1)$$

Further introducing $m = (M_{\mathrm{ab}}/M_0)$, Eq. (1) shows that a plot of η against m^2 should yield a straight line with κ_1 as

the intercept. Even though this "Sucksmith-Thompson method" was derived for ferromagnets, the technical procedure of plotting η against m^2 can also be performed for ferrimagnets like $GdCo_5$ [26,29]. In this case, the quantity extracted from the intercept is an effective anisotropy constant $K_{\rm eff}$ so, unlike YCo_5, the anisotropy constants reported in Refs. [26,29] are distinct from the κ_1 values extracted from Fig. 1. As recognized at the time of the original experiments [27–30], the reduced value of $K_{\rm eff}$ with respect to κ_1 of YCo_5 is a fingerprint of canting between the Gd and Co sublattices.

Making contact with previous experiments, thus, requires that we obtain $K_{\rm eff}$. To this end, we have developed a scheme of calculating first-principles hard-plane magnetization versus field curves, on which we perform the Sucksmith-Thompson analysis to directly mirror the experiments. The central concept of FPMVB is that at equilibrium, the torques from the exchange, spin-orbit, and dipole interactions must balance those arising from the external field. Then,

$$B = \frac{\partial F(T)}{\partial \theta_i} \frac{1}{M_i \cos\theta_i + \sum_j \sin\theta_j \frac{\partial M_j}{\partial \theta_i}}. \qquad (2)$$

The magnetization at a given B, T is determined by the angle set $\{\theta_{\rm Gd}, \theta_{\rm Co_1}, \theta_{\rm Co_2}, \ldots\}$, which satisfies Eq. (2) for every magnetic sublattice. The spin-orbit interaction breaks the symmetry of the Co_{3g} atoms such that, altogether, there are four independent angles to vary for $GdCo_5$. The second term in the denominator of Eq. (2) reflects that the magnetic moments themselves might depend on θ_i (magnetization anisotropy). We have tested (i) neglecting this contribution, and (ii) modeling the dependence as $M_i(\theta_i) = M_{0i}(1 - p_i \sin^2\theta_i)$, where M_{0i} and p_i are parametrized from our calculations.

Figure 2 shows FPMVB curves of $GdCo_5$ calculated using Eq. (2) with methods (i) and (ii) (crosses and circles), which yield virtually identical values of $K_{\rm eff}$. The M versus B curves in the left panel resemble those of a ferromagnet where, as the temperature increases, it becomes easier to rotate the moments away from the easy axis so that a given B field induces a larger magnetization. However, plotting η against m^2 in the right panel tells a more interesting story. The effective anisotropy constant $K_{\rm eff}$ (y-axis intercept) at 0 K is 1.53 meV, much smaller than κ_1 of YCo_5. Furthermore, $K_{\rm eff}$ increases with temperature, to 1.74 meV at 300 K. Therefore, in contrast to the standard calculations of Fig. 1, the FPMVB approach reproduces the experimental behavior of Refs. [26,29].

Our FPMVB calculations provide a microscopic insight into the magnetization process. For instance, at 0 K and 9 T, we calculate that the cobalt moments rotate away from the easy axis by 6.1°. By contrast, the Gd moments have rotated by only 3.9°; i.e., the ideal 180° Gd-Co alignment has reduced by 2.2° (the geometry is shown in Fig. 2). We also

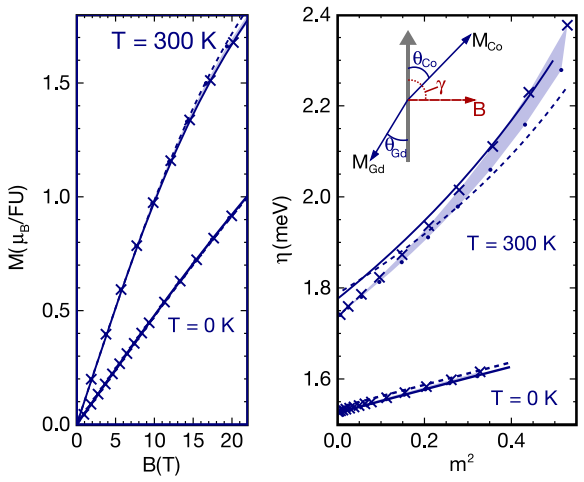

FIG. 2. Magnetization of $GdCo_5$ vs applied magnetic field shown on a standard plot (left panel) or after the Sucksmith-Thompson analysis [Eq. (1), right panel]. Crosses/circles are calculated with methods (i)/(ii) discussed in the text, and the area between them shaded as a guide to the eye. Note the two methods are effectively indistinguishable in the left panel. The dashed/solid lines are calculated from the model free energies F_1 and F_2. The right panel also shows the geometry of the magnetization and field with respect to the crystallographic c-axis (thick gray arrow).

find canting between the different Co sublattices, but not by more than 0.1° at both 0 and 300 K (the calculated angles as a function of field are shown in the SM [48]). This Co-Co canting is small, thanks to the Co-Co ferromagnetic exchange interaction remaining strong over a wide temperature range [44]. The temperature dependence of $K_{\rm eff}$ can be traced to the fact that the easy axis magnetization M_0 of $GdCo_5$ initially increases with temperature [44]. Even if $M_{\rm ab}$ increases with temperature at a given field, a faster increase in M_0 can lead to an overall hardening in $K_{\rm eff}$ [Eq. (1)].

We assign the canting in $GdCo_5$ to a delicate competition between the exchange interaction favoring antiparallel Co/Gd moments, uniaxial anisotropy favoring c-axis (anti)alignment, and the external field trying to rotate all moments into the hard plane. We can quantify these interactions by looking for a model parametrization of the free energy F. Crucially, we can train the model with an arbitrarily large set of first-principles calculations exploring sublattice orientations not accessible experimentally, and test its performance against the torque calculations of Eq. (2). Neglecting the 0.1° canting within the cobalt sublattices gives two free angles, $\theta_{\rm Gd}$ and $\theta_{\rm Co}$. Including the Gd-Co exchange A, uniaxial Co anisotropy $K_{1,\rm Co}$, and a dipolar contribution $S(\theta_{\rm Gd}, \theta_{\rm Co})$ [31,48] leads naturally to a two-sublattice model [30],

$$F_1(\theta_{\rm Gd}, \theta_{\rm Co}) = -A\cos(\theta_{\rm Gd} - \theta_{\rm Co}) + K_{1,\rm Co}\sin^2\theta_{\rm Co} + S(\theta_{\rm Gd}, \theta_{\rm Co}). \qquad (3)$$

The training calculations showed additional angular dependences not captured by F_1, so we also investigated:

$$F_2(\theta_{\mathrm{Gd}},\theta_{\mathrm{Co}}) = F_1(\theta_{\mathrm{Gd}},\theta_{\mathrm{Co}}) + K_{2,\mathrm{Co}}\sin^4\theta_{\mathrm{Co}} + K_{1,\mathrm{Gd}}\sin^2\theta_{\mathrm{Gd}}. \quad (4)$$

As discussed below the training calculations showed no strong evidence of Gd-Co exchange anisotropy [31–34].

The dashed (solid) lines in Fig. 2 are the calculated M versus B curves obtained by minimizing $F_{1(2)} - \sum_i \boldsymbol{M_i}\cdot\boldsymbol{B}$. The second term includes magnetization anisotropy on the cobalt moments [48,57]. On the scale of the left panel, both F_1 and F_2 give excellent fits to the torque calculations, especially up to moderate fields. The plot of η against m^2 reveals some differences, with F_2 giving a marginally improved description of the data, but F_1 already captures the most important physics.

We also applied the FPMVB approach to YCo_5, using Eq. (2) and the model for F introduced in Ref. [57]. Then, parametrizing the models [48] over the temperature range 0–400 K, calculating M versus B curves, and extracting K_{eff} using the Sucksmith-Thompson plots gives the results shown in the left panel of Fig. 3. We also show κ_1 of $GdCo_5$ to emphasize the difference between FPMVB calculations and the "standard" ones of Fig. 1.

Comparing K_{eff} to previously-published experimental measurements on $GdCo_5$ raises some issues. First, the three studies in the literature report anisotropy constants that differ by as much as 1 meV [26,29,58]. Indeed, there was controversy over whether the observed results were evidence of an anisotropic exchange interaction between Gd and Co [31,32] or an artifact of poor sample stoichiometry [33,34]. Furthermore, the only study performed above room temperature [26] reports, without comment, some peculiar behavior where K_{eff} of $GdCo_5$ exceeds that of YCo_5 at high temperature [28], despite conventional wisdom that the half filled $4f$ shell of Gd does not contribute to the anisotropy.

Our calculations do in fact show an excess in the rigid-moment anisotropy of $GdCo_5$ of 16% at 0 K (Fig. 1) compared to YCo_5. The authors of Refs. [29,31] fitted their experimental data with a much larger excess of 50%, while the high-field study of Ref. [33] found (11 ± 15)%, with the authors of that work attributing the difference to an improved sample stoichiometry [34]. Our calculated excess at 0 K is formed from two major contributions: the dipole interaction energy, which accounts for 0.31 meV/FU, and $K_{1,\mathrm{Gd}}$ [Eq. (4)], which we found to be 24% the size of $K_{1,\mathrm{Co}}$. The nonzero value of $K_{1,\mathrm{Gd}}$ is due to the $5d$ electrons, whose presence is evident from the Gd magnetization (7.47 μ_B at 0 K). We did not find a significant contribution from anisotropic exchange, which we tested in two ways: first by attempting to fit a term $A(1 - p'\sin^2\theta_{\mathrm{Co}})\cos(\theta_{\mathrm{Gd}} - \theta_{\mathrm{Co}})$ to our training set of calculations, and also by computing Curie temperatures

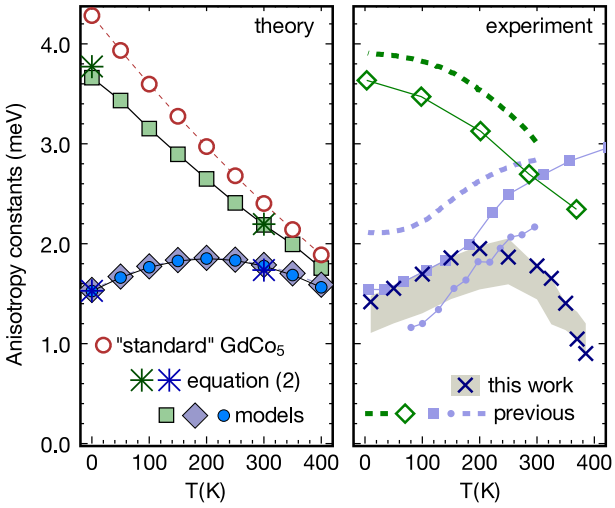

FIG. 3. Anisotropy constants K_{eff} vs. temperature of YCo_5 (green) and $GdCo_5$ (blue). The left panel shows calculations using Eq. (2) at 0 and 300 K (stars), or using parameterized model expressions F_1 (diamonds) and F_2 (circles), and from Ref. [57] (YCo_5, squares). For $GdCo_5$ we also show in red κ_1 extracted from "standard" calculations where the Gd and Co moments were held rigidly antiparallel (cf. Fig. 1). The experimental data in the right panel were measured by us for $GdCo_5$ (crosses, with shaded background) or taken from Refs. [26,29,58] (squares, dashed lines, circles) and Refs [28,51] (green diamonds and dashed lines, YCo_5).

with the (rigidly antiparallel) magnetization directed either along the c or a axes. We found the magnitude of the anisotropy (p') to be smaller than 0.5%, negative at 0 K, and to decrease in magnitude as the temperature is raised. Consistently, the Curie temperature was found to be only 1 K higher for a axis alignment, which we do not consider significant.

However, our calculations do not predict the K_{eff} value of $GdCo_5$ to exceed YCo_5. Indeed, in Fig. 3, κ_1 of $GdCo_5$ approaches that of YCo_5 at high temperatures, which is significant because κ_1 provides an upper bound for K_{eff} [32]. To resolve this final puzzle, we performed our own measurements of K_{eff} on the single crystal, whose growth we reported recently [44]. Hard and easy axis magnetization curves up to 7 T were measured in a Quantum Design superconducting quantum interference device (SQUID) magnetometer, and the anisotropy constants were extracted from Sucksmith-Thompson plots [48]. The right panel of Fig. 3 shows our newly measured data as crosses. Previously reported measurements are shown in faint blue or green for $GdCo_5$ [26,29,58] or YCo_5 [28,51].

Up to 200 K, there is close agreement between the experiments of Ref. [26], our own experiments, and the FPMVB calculations. Above this temperature, our new experiments show the expected drop in K_{eff}, while the previously reported data show a continued rise [26]. We repeated our measurements using different protocols and found a reasonably large variation in the extracted K_{eff} [48].

Even taking this variation into account as the shaded area in Fig. 3, the drop is still observed.

We therefore do not believe the high temperature behavior reported in Ref. [26] has an intrinsic origin. Possible extrinsic factors include the method of sample preparation, degradation of the $RECo_5$ phase at elevated temperatures [59], and potential systematic error when extracting K_{eff}. We note that even the idealized theoretical curves in Fig. 2 show curvature at higher temperature, making it more difficult to find the intercept.

In conclusion, we have introduced the FPMVB approach to interpret experiments measuring anisotropy of ferrimagnets, particularly RE-TM permanent magnets. We presented the method in the context of our DLM formalism, but any electronic structure theory capable of calculating magnetic couplings relativistically [60–64] should be able to produce FPMVB curves, at least at zero temperature. However, standard calculations that neglect the external field should be used with care when comparing to experiments on ferrimagnets. Similarly, the prototype $GdCo_5$ serves as a reminder that a simple view of the anisotropy energy does not fully describe the magnetization processes in ferrimagnets, which might have implications in understanding, e.g., magnetization reversal in nanomagnetic assemblies [65]. Overall, our Letter demonstrates the benefit of interconnected computational and experimental research in this key area.

The present work forms part of the PRETAMAG project, funded by the UK Engineering and Physical Sciences Research Council (EPSRC), Grant No. EP/M028941/1. Crystal growth work at Warwick is also supported by EPSRC Grant No. EP/M028771/1. Work at Daresbury Laboratory was supported by an EPSRC service level agreement with the Scientific Computing Department of STFC. We thank E. Mendive-Tapia for useful discussions and A. Vasylenko for continued assistance in translating references.

*c.patrick.1@warwick.ac.uk

[1] S. Chikazumi, *Physics of Ferromagnetism*, 2nd ed. (Oxford University Press, New York, 1997).
[2] H. Kronmüller, Phys. Status Solidi B **144**, 385 (1987).
[3] P. Strange, *Relativistic Quantum Mechanics* (Cambridge University Press, Cambridge, 1998).
[4] K. Strnat, G. Hoffer, J. Olson, W. Ostertag, and J. J. Becker, J. Appl. Phys. **38**, 1001 (1967).
[5] O. Gutfleisch, M. A. Willard, E. Brück, C. H. Chen, S. G. Sankar, and J. P. Liu, Adv. Mater. **23**, 821 (2011).
[6] M. Sagawa, S. Fujimura, N. Togawa, H. Yamamoto, and Y. Matsuura, J. Appl. Phys. **55**, 2083 (1984).
[7] J. J. Croat, J. F. Herbst, R. W. Lee, and F. E. Pinkerton, J. Appl. Phys. **55**, 2078 (1984).
[8] J. M. D. Coey, IEEE Trans. Magn. **47**, 4671 (2011).
[9] R. Skomski, P. Manchanda, P. Kumar, B. Balamurugan, A. Kashyap, and D. J. Sellmyer, IEEE Trans. Magn. **49**, 3215 (2013).
[10] M. D. Kuz'min and A. M. Tishin, in *Handbook of Magnetic Materials*, edited by K. H. J. Buschow (Elsevier B.V., New York, 2008) Vol. 17, Chap. 3, p. 149.
[11] Z. Tie-song, J. Han-min, G. Guang-hua, H. Xiu-feng, and C. Hong, Phys. Rev. B **43**, 8593 (1991).
[12] M. Richter, J. Phys. D **31**, 1017 (1998).
[13] M. D. Kuz'min, Y. Skourski, D. Eckert, M. Richter, K.-H. Müller, K. P. Skokov, and I. S. Tereshina, Phys. Rev. B **70**, 172412 (2004).
[14] P. Delange, S. Biermann, T. Miyake, and L. Pourovskii, Phys. Rev. B **96**, 155132 (2017).
[15] L. Steinbeck, M. Richter, and H. Eschrig, J. Magn. Magn. Mater. **226–230**, 1011 (2001).
[16] P. Larson, I. I. Mazin, and D. A. Papaconstantopoulos, Phys. Rev. B **69**, 134408 (2004).
[17] H. Pang, L. Qiao, and F. S. Li, Phys. Status Solidi B **246**, 1345 (2009).
[18] M. Matsumoto, R. Banerjee, and J. B. Staunton, Phys. Rev. B **90**, 054421 (2014).
[19] A. Landa, P. Söderlind, D. Parker, D. Åberg, V. Lordi, A. Perron, P. E. A. Turchi, R. K. Chouhan, D. Paudyal, and T. A. Lograsso, arXiv:1707.09447.
[20] O. Eriksson, B. Johansson, R. C. Albers, A. M. Boring, and M. S. S. Brooks, Phys. Rev. B **42**, 2707 (1990).
[21] H. Eschrig, M. Sargolzaei, K. Koepernik, and M. Richter, Europhys. Lett. **72**, 611 (2005).
[22] G. H. O. Daalderop, P. J. Kelly, and M. F. H. Schuurmans, Phys. Rev. B **53**, 14415 (1996).
[23] J. B. Staunton, S. Ostanin, S. S. A. Razee, B. L. Gyorffy, L. Szunyogh, B. Ginatempo, and E. Bruno, Phys. Rev. Lett. **93**, 257204 (2004).
[24] K. Kumar, J. Appl. Phys. **63**, R13 (1988).
[25] K. Buschow, A. van Diepen, and H. de Wijn, Solid State Commun. **15**, 903 (1974).
[26] A. Ermolenko, IEEE Trans. Magn. **12**, 992 (1976).
[27] S. Rinaldi and L. Pareti, J. Appl. Phys. **50**, 7719 (1979).
[28] A. S. Yermolenko, Phys. Met. Metallogr. **50**, 741 (1980).
[29] R. Ballou, J. Déportes, B. Gorges, R. Lemaire, and J. Ousset, J. Magn. Magn. Mater. **54–57**, 465 (1986).
[30] R. Radwański, Physica (Amsterdam) **142B+C**, 57 (1986).
[31] R. Ballou, J. Déportes, and J. Lemaire, J. Magn. Magn. Mater. **70**, 306 (1987).
[32] P. Gerard and R. Ballou, J. Magn. Magn. Mater. **104–107**, 1463 (1992).
[33] R. Radwański, J. Franse, P. Quang, and F. Kayzel, J. Magn. Magn. Mater. **104–107**, 1321 (1992).
[34] J. J. M. Franse and R. J. Radwański, in *Handbook of Magnetic Materials*, edited by K. H. J. Buschow (Elsevier North-Holland, New York, 1993) Vol. 7, Chap. 5, p. 307.
[35] T. Zhao, H. Jin, R. Grössinger, X. Kou, and H. R. Kirchmayr, J. Appl. Phys. **70**, 6134 (1991).
[36] B. L. Györffy, A. J. Pindor, J. Staunton, G. M. Stocks, and H. Winter, J. Phys. F **15**, 1337 (1985).
[37] J. B. Staunton, L. Szunyogh, A. Buruzs, B. L. Gyorffy, S. Ostanin, and L. Udvardi, Phys. Rev. B **74**, 144411 (2006).
[38] We performed a sum over dipoles [1] using the calculated $\boldsymbol{M}_i(T)$ out to a radius of 20 nm.

[39] E. Bruno and B. Ginatempo, Phys. Rev. B **55**, 12946 (1997).
[40] P. Strange, J. Staunton, and B. L. Gyorffy, J. Phys. C **17**, 3355 (1984).
[41] M. Däne, M. Lüders, A. Ernst, D. Ködderitzsch, W. M. Temmerman, Z. Szotek, and W. Hergert, J. Phys. Condens. Matter **21**, 045604 (2009).
[42] S. H. Vosko, L. Wilk, and M. Nusair, Can. J. Phys. **58**, 1200 (1980).
[43] M. Lüders, A. Ernst, M. Däne, Z. Szotek, A. Svane, D. Ködderitzsch, W. Hergert, B. L. Györffy, and W. M. Temmerman, Phys. Rev. B **71**, 205109 (2005).
[44] C. E. Patrick, S. Kumar, G. Balakrishnan, R. S. Edwards, M. R. Lees, E. Mendive-Tapia, L. Petit, and J. B. Staunton, Phys. Rev. Mater. **1**, 024411 (2017).
[45] H. Ebert and M. Battocletti, Solid State Commun. **98**, 785 (1996).
[46] H. Ebert, Fully relativistic band structure calculations for magnetic solids—formalism and application, in *Electronic Structure and Physical Properties of Solids: The Uses of the LMTO Method Lectures of a Workshop Held at Mont Saint Odile, France, October 2–5,1998*, edited by H. Dreyssé (Springer Berlin Heidelberg, Berlin, 2000) pp. 191–246.
[47] L. Steinbeck, M. Richter, and H. Eschrig, Phys. Rev. B **63**, 184431 (2001).
[48] See Supplemental Material at http://link.aps.org/supplemental/10.1103/PhysRevLett.120.097202 for further experimental and computational details, description of the orbital polarization correction, discussion of magnetization anisotropy, the parameters used to simulate MvB curves, and the angle sets that satisfy Eq. (2).
[49] G. H. O. Daalderop, P. J. Kelly, and M. F. H. Schuurmans, Phys. Rev. B **41**, 11919 (1990).
[50] X. Wang, R. Wu, D.-s. Wang, and A. J. Freeman, Phys. Rev. B **54**, 61 (1996).
[51] J. M. Alameda, D. Givord, R. Lemaire, and Q. Lu, J. Appl. Phys. **52**, 2079 (1981).
[52] H. Klein, A. Menth, and R. Perkins, Physica (Amsterdam) **80B+C**, 153 (1975).
[53] K. H. J. Buschow and F. R. de Boer, *Physics of Magnetism and Magnetic Materials* (Springer, Boston, 2003).
[54] A. Paoluzi, L. Pareti, M. Solzi, and F. Albertini, J. Magn. Magn. Mater. **132**, 185 (1994).
[55] Y. Wang, Y. Zhao, S. Wang, M. Lu, H. Zhai, Y. Zhai, K. Shono, and X. Yu, J. Appl. Phys. **93**, 7789 (2003).
[56] W. Sucksmith and J. E. Thompson, Proc. R. Soc. A **225**, 362 (1954).
[57] J. Alameda, J. Déportes, D. Givord, R. Lemaire, and Q. Lu, J. Magn. Magn. Mater. **15–18**, 1257 (1980).
[58] T. Katayama, M. Ohkoshi, Y. Koizumi, T. Shibata, and T. Tsushima, Appl. Phys. Lett. **28**, 635 (1976).
[59] F. Den Broeder and K. Buschow, J. Less-Common Met. **29**, 65 (1972).
[60] L. Udvardi, L. Szunyogh, K. Palotás, and P. Weinberger, Phys. Rev. B **68**, 104436 (2003).
[61] H. Ebert and S. Mankovsky, Phys. Rev. B **79**, 045209 (2009).
[62] J. Hu and R. Wu, Phys. Rev. Lett. **110**, 097202 (2013).
[63] S. Ayaz Khan, P. Blaha, H. Ebert, J. Minár, and O. Šipr, Phys. Rev. B **94**, 144436 (2016).
[64] M. Hoffmann, B. Zimmermann, G. P. Müller, D. Schürhoff, N. S. Kiselev, C. Melcher, and S. Blügel, Nat. Commun. **8**, 308 (2017).
[65] Z. J. Guo, J. S. Jiang, J. E. Pearson, S. D. Bader, and J. P. Liu, Appl. Phys. Lett. **81**, 2029 (2002).